Radio Science, Volume 32, Number 2, Pages 305–315, March–April 1997

Zero-order time domain scattering of electromagnetic plane waves by two quarter spaces

Edson E. S. Sampaio

Programa de Pesquisa e Pós-Graduação em Geofísica, Instituto de Geociências da Universidade Federal da Bahia, Salvador, Brazil

Mikhail M. Popov

V. A. Steklov Mathematical Institute, St. Petersburg, Russia

Abstract. The zero-order term of the time domain scattered electric field of an electromagnetic plane wave normally incident upon the surface of two quarter spaces is determined. The general solution is a development from a previous exact and complete solution in the frequency domain. The zero-order term of the scattered electric field has been computed in the upper medium ($z < 0$). The incident wave in the frequency domain assumes the same function for three cases: (1) The conductivity vanishes everywhere; (2) only the conductivity of the upper medium is zero; and (3) the three media are conductors. Case 1 helps to understand cases 2 and 3. Case 2 is applicable to geophysical exploration. For cases 1 and 2 a causal time function decaying exponentially with time at every point above the fault ($z < 0$) describes the waveform of the incident plane wave. The zero-order term of the scattered field has been computed above the fault. At $x = 0$ it reduces to a closed expression for case 1 and to a single integral for the other two cases. In the three cases it contains an integral of a Hankel function for $x \neq 0$. The computation of the high-frequency part of the inverse Fourier transform for $x \neq 0$ employs asymptotic expressions for the Hankel function using analytical techniques of the geometrical theory of diffraction for cases 1 and 2. For case 3 the inverse Fourier transform may have two possible contributions: either from the residue at a single pole or from the integral along a branch cut in the ω plane. The wave front of the scattered field is well defined in shape, phase, and amplitude. Its amplitude is discontinuous at $x = 0$, and varies smoothly but presents a sharp jump for $| x | << | z |$. For $| x | = O(z)$, there is a numerical noise that oscillates at 100 MHz.

Introduction

Given the large variation of the value of the electrical conductivity in Earth materials, the electromagnetic methods present a degree of discrimination higher than the seismic methods. Therefore there is much interest in applying the electromagnetic methods, where the seismic methods break down, as in the investigation of structures below volcanics or evaporites. So the investigation of the scattering of electromagnetic waves by sharp lateral variation of electrical conductivity is fundamental for geophysical exploration. It is also important in other areas involving the propagation of electromagnetic waves, as communications and Global Positioning Systems. The electromagnetic plane wave scattering by a vertical fault represents the simplest model of geophysical interest related to two-dimensional scattering of plane waves. Here we face the classical problem of scattering by a penetrable wedge. As it became evident after years of intensive efforts, this problem cannot be solved in closed analytical form. Otherwise, it could provide a rigorous mathematical analysis of the wave phenomenon, as it has happened for the problem of diffraction of a plane wave by a conductive half plane [*Sommerfeld*, 1896].

Paper number 96RS03201.
0048-6604/97/96RS-03201$11.00

Finite element and finite difference methods can be used for obtaining approximate solutions to this and more complicated forward modeling problems. These techniques are accurate for sufficiently small steps and sizes of the meshes, but they quickly become very time consuming with the increase of both time and distance from the scatter to the point of observation. They also lack a physical insight of the involved boundary problem, particularly at infinity. The ray method usually contains a detailed picture of waves involved in the process. For this case it fails due to inability to find diffraction coefficients for the wave reradiated by the fault.

The objective of the present paper is to study the wedge problem for the case of vertical faults, based on integral equations and subsequent perturbation theory for them in the time domain. We consider not only the geometry but also the physical properties of the three media that compose the fault models. The models under consideration are simple, but they represent an approximation to the real world in certain cases, and our basic treatment of the problem is rigorous. It also can be used to check the degree of precision of other techniques.

Sampaio and Fokkema [1992] developed a complete and exact solution to this problem in the frequency domain. In the present paper we adapt their solution to find the scattered field in the time domain caused by a normally incident plane wave, represented by a causal time function that decays exponentially with time of propagation from a height of reference above the fault. We selected the zero-order term of the expansion and computed the corresponding approximate scattered electric field component above the fault, considering the upper medium to be free space (cases 1 and 2).

For the selected zero-order approximation we obtain analytical expressions for the wave field in terms of integrals with oscillating functions (in ω domain). Using analytical techniques well known in GTD (geometrical theory of diffraction), in particular, the stationary phase method, we derive high-frequency asymptotics for those integrals. This asymptotic approach enables us to retrieve the geometrical picture of the waves involved in the process under consideration and allows us to simplify numerical computations of the double integral for the scattered field.

Statement of the Problem

An electromagnetic plane wave propagates in the positive z direction and normally impinges on the surface of two quarter spaces as depicted in Figure 1. We assume that the electric and the magnetic field components of the wave are horizontal and orthogonal to each other, with the electric field parallel to the strike of the vertical plane that separates the two quarter spaces, and that the phase velocity of the wave has a finite and distinct value in each medium. The problem consists of solving the two-dimensional wave equation in the frequency domain for each medium,

$$\left(\partial_x^2 + \partial_z^2 + \kappa_n^2\right) E_n(x, z, \omega) = 0, \tag{1}$$

where $\kappa_n = \sqrt{\omega^2 \mu_n \epsilon_n - i\omega\mu_n\sigma_n}$, $\Im(\kappa_n) \leq 0$, $n = 0, 1, 2$. Two sets of boundary conditions have to be satisfied at each interface: (1) continuity of the horizontal electric field and (2) continuity of the tangential component of the magnetic field. In equation (1), $E_n(x, z, \omega)$ and ω represent the electric field and the angular frequency, respectively, μ_n is the magnetic permeability, ϵ_n is the dielectric permittivity, and σ_n is the electric conductivity of the nth medium.

The primary incident electric field, $E_0^I(z, \omega)$, exists only in the medium 0 (for $z < 0$), satisfies the one-dimensional wave equation,

$$\left(\partial_z^2 + \kappa_0^2\right) E_0^I(z, \omega) = 0, \tag{2}$$

and may be given by

$$E_0^I(z, \omega) = A(\omega)\, e^{-i\kappa_0 z}, \tag{3}$$

where we assume that

$$A(\omega) = \frac{N(\omega)}{a + i\omega}\, e^{-i\kappa_0 h}, \tag{4}$$

$$N(\omega) = \frac{2\mu_0\omega\sqrt{\mu_v\epsilon_v}}{\left(\mu_v\sqrt{\mu_0\epsilon_0}\sqrt{\omega(\omega - i\tilde{\sigma}_0)} + \mu_0\omega\sqrt{\mu_v\epsilon_v}\right)},$$

$$\tilde{\sigma}_n = \frac{\sigma_n}{\epsilon_n}, \quad n = 0, 1, 2.$$

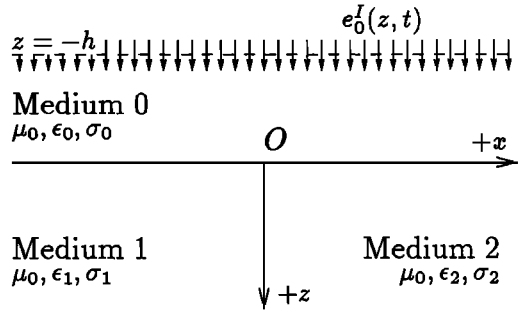

Figure 1. Configuration of the incident field and the fault model.

In (4), $h > 0$ is a height of reference above the surface, a is a real positive number having the dimension of frequency, and the subscript v refers either to the free space or to the air. $A(\omega)$ has one pole at $\omega = ia$ and two branch points at $\omega = 0$ and $\omega = i\tilde{\sigma}_0$. If medium 0 is not the air, the representation of $A(\omega)$ assumes that the interface between medium 0 and the air is sufficiently distant, not to be reached by either the reflected or the scattered field during the time interval of investigation. If medium 0 is the air, we can approximate $\kappa_0 = \omega/c$, where c is the velocity of the electromagnetic wave in free space. In this case the primary electric field in the time domain is given by

$$e_0^I(z,t) = \mathcal{H}(t - \frac{z+h}{c})\, e^{-a(t-\frac{z+h}{c})}, \qquad (5)$$

where $\mathcal{H}(\psi)$ is the Heaviside step function. However, if medium 0 is a good conductor, the primary electric field must be written as

$$e_0^I(z,t) = \frac{1}{\pi}\,\Re\left(\int_0^\infty A(\omega) e^{-i\kappa_0 z + i\omega t}\, d\omega\right). \qquad (6)$$

Appendices A, B, and C contain a thorough analysis of equation (6).

Zero-Order Field in the Upper Medium

From here on we will analyze and compute the field only in the upper medium (for $z < 0$). We will employ the representation given by *Sampaio and Fokkema* [1992] for the electric field in the frequency domain, with the change introduced by *Sampaio and Popov* [1996] for the acoustic field. Taking only the first term (zero-order term) of the series representation of the scattered component, we have

$$E_{0,1}(x,z,\omega) = A(\omega)\left(e^{-i\kappa_0 z} + \frac{c_1-1}{c_1+1} e^{+i\kappa_0 z}\right) - E_{s,0}^{(0)}(x,z,\omega),\ x<0\ z<0, \qquad (7)$$

$$E_{0,2}(x,z,\omega) = A(\omega)\left(e^{-i\kappa_0 z} + \frac{c_2-1}{c_2+1} e^{+i\kappa_0 z}\right) + E_{s,0}^{(0)}(x,z,\omega),\ x>0\ z<0. \qquad (8)$$

The zero-order scattered electric field in the frequency domain in $z < 0$ is given by

$$E_{s,0}^{(0)}s(x,z,\omega) = \frac{i\kappa_0 A(\omega) C_{2,1}}{2\pi} \int_{-\infty}^{+\infty} \frac{e^{-u_0|x| + i\alpha z}}{u_0^2}\, d\alpha, \qquad (9)$$

$$u_0 = \sqrt{\alpha^2 - \kappa_0^2},\quad \Re(u_0) > 0,$$

$$c_n = \frac{\mu_n \kappa_0}{\mu_0 \kappa_n},\ n = 1,2, \qquad (10)$$

$$C_{2,1} = \left(\frac{c_1-1}{c_1+1} - \frac{c_2-1}{c_2+1}\right). \qquad (11)$$

The path of integration of (9) and the branch cuts on the complex α plane are represented in Figure 2, assuming that medium 0 is free space. If medium 0 is a conductive medium, the path of integration will correspond to the real axis, because the branch cuts may be chosen not to intersect it. Therefore we can express the real function $e_{s,0}^{(0)}(x,z,t)$ in the following form:

$$e_{s,0}^{(0)}(x,z,t) = \frac{1}{4\pi^2} \int_{-\infty}^{+\infty} i\kappa_0 C_{2,1} A(\omega) e^{i\omega t} \times \left(\int_{-\infty}^{+\infty} \frac{e^{-\sqrt{\alpha^2-\kappa_0^2}|x| + i\alpha z}}{\alpha^2 - \kappa_0^2} d\alpha\right) d\omega. \qquad (12)$$

Zero-Order Scattered Electric Field for x = 0

Equations (7) and (8) show that the zero-order scattered electric feld is odd with respect to x and discontinuous at $x = 0$. For $x = 0$ the branch cuts of (9) disappear. So we can close the contour in the lower half plane of α as shown in Figure 3, and therefore

$$\int_{-\infty}^{+\infty} \frac{e^{i\alpha z}}{\alpha^2 - (\kappa_0)^2}\, d\alpha = -\frac{\pi i}{\kappa_0} e^{+i\kappa_0 z},\ z<0.$$

Substituting this result in (12) we obtain

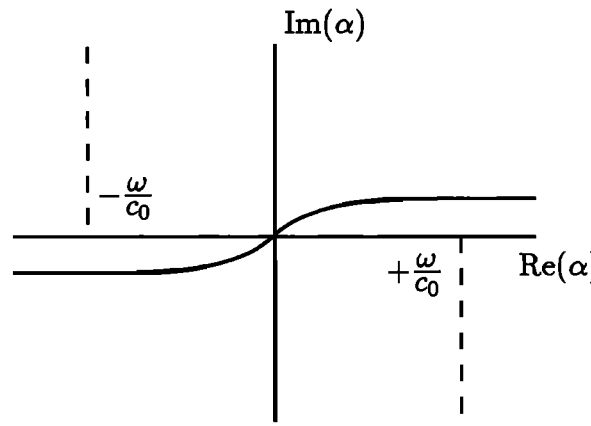

Figure 2. Path of integration and the branch cuts of the α plane for $x \neq 0$ and $\sigma_0 = 0$.

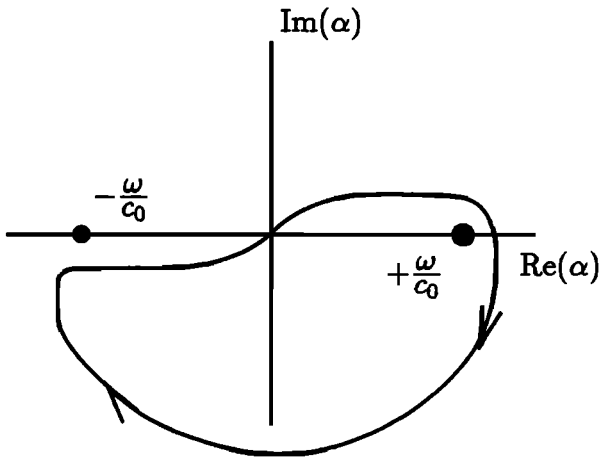

Figure 3. Path of integration and the poles of the α plane for $x = 0$ and $\sigma_0 = 0$.

$$e^{(0)}_{s,0}(0,z,t) = \frac{1}{2\pi}\Re\left(\int_0^{+\infty} C_{2,1}A(\omega)e^{i\omega t + i\kappa_0 z}\,d\omega\right). \tag{13}$$

If the three media are nonconductive, (13) reduces to

$$e^{(0)}_{s,0}(0,z,t) = \frac{C_{2,1}}{2}\mathcal{H}(t+\frac{z-h}{c})\,e^{-a(t+\frac{z-h}{c})}. \tag{14}$$

Zero-Order Scattered Electric Field for $x \neq 0$

According to *Erdélyi* [1954],

$$\int_{-\infty}^{+\infty} \frac{e^{-\sqrt{\alpha^2-(\kappa_0)^2}|x|+i\alpha z}}{\sqrt{\alpha^2-(\kappa_0)^2}}\,d\alpha = -\pi i H_0^{(2)}(\kappa_0\sqrt{x^2+z^2}).$$

Therefore the scattered electric field assumes the following expression for $x \neq 0$:

$$e^{(0)}_{s,0}(x,z,t) = e^{(0)}_{s,0}(0,z,t) - \frac{1}{4\pi}\int_{-\infty}^{+\infty} \kappa_0 C_{2,1}A(\omega)\,I(x,z,\omega)e^{i\omega t}\,d\omega, \tag{15}$$

where

$$I(x,z,\omega) = \int_0^{|x|} H_0^{(2)}\left(\kappa_0\sqrt{\eta^2+z^2}\right)d\eta.$$

Nonconductive Upper Half Space

For this case, $\sigma_0 = 0$ and $\kappa_0 = \omega/c$. We assume that $\mu_0 = 4\pi \times 10^{-7}$ henries/m, and that $\epsilon_0 = \frac{1}{36\pi} \times 10^{-9}$ F/m. For nonconductive lower media, $\sigma_1 = \sigma_2 = 0$. Under those circumstances, c_1, c_2, and $C_{2,1}$ are real and independent of frequency. Let $\mu_1 = \mu_2 = \mu_0$, $\epsilon_1 = 4\epsilon_0$, and $\epsilon_2 = 81\,\epsilon_0$. This is approximately the case when medium 0 is the air, medium 1 is a dry sandstone, and medium 2 is pure water. We verify at once that $c_1 = 0.5$, $c_2 = 1/9$,

$$e^{(0)}_{0,1}(x,z,t) = \mathcal{H}(t^-)e^{-at^-} - 0.8\mathcal{H}(t^+)e^{-at^+} - e^{(0)}_{s,0}(x,z,t), \tag{16}$$

and

$$e^{(0)}_{0,2}(x,z,t) = \mathcal{H}(t^-)e^{-at^-} - \frac{1}{3}\mathcal{H}(t^+)e^{-at^+} + e^{(0)}_{s,0}(x,z,t), \tag{17}$$

where $t^- = t + (|z|-h)/c$, and $t^+ = t - (|z|+h)/c$. Here $e^{(0)}_{s,0}(x,z,t)$ is given by (15), with $C_{2,1} = +7/15$, and $e^{(0)}_{s,0}(0,z,t)$ given by (14). Also,

$$A(\omega) = \frac{e^{-i\omega\frac{h}{c}}}{a+i\omega}. \tag{18}$$

Let us assume that for the conductive lower-media case ($\sigma_1 \neq \sigma_2 \neq 0$), we also have that $\epsilon_0 = \epsilon_1 = \epsilon_2$. In this case, $\kappa_n^2 = \mu_0\epsilon_n\omega(\omega - i\tilde{\sigma}_n)$, $n = 1,2$. This implies that $c_1 = c_2 = C_{2,1} = 0$ for $\omega = 0$;

$$c_n = \frac{\omega}{\sqrt{\omega(\omega - i\tilde{\sigma}_n)}},\ n = 1,2;$$

and consequently that

$$C_{2,1} = \frac{\omega - \sqrt{\omega(\omega - i\tilde{\sigma}_1)}}{\omega + \sqrt{\omega(\omega - i\tilde{\sigma}_1)}} - \frac{\omega - \sqrt{\omega(\omega - i\tilde{\sigma}_2)}}{\omega + \sqrt{\omega(\omega - i\tilde{\sigma}_2)}}. \tag{19}$$

Therefore

$$e^{(0)}_{0,1}(x,z,t) = \mathcal{H}(t^-)\,e^{-at^-} + e^{(R)}_{0,1}(z,t) - e^{(0)}_{s,0}(x,z,t), \tag{20}$$

and

$$e^{(0)}_{0,2}(x,z,t) = \mathcal{H}(t^-)\,e^{-at^-} + e^{(R)}_{0,2}(z,t) + e^{(0)}_{s,0}(x,z,t). \tag{21}$$

Here $e^{(0)}_{s,0}(x,z,t)$ is given by (15), with $A(\omega)$ given by (18) and $C_{2,1}$ given by (19), and

$$e^{(R)}_{0,n}(z,t) = \frac{1}{\pi}\Re\left(\int_0^{\infty} \frac{c_n - 1}{c_n + 1}\,\frac{e^{i\omega t^+}}{a+i\omega}\,d\omega\right),\ n = 1,2. \tag{22}$$

Appendix D contains a thorough investigation of (22).

Three Conductive Media

Let $\kappa_j^2 = \mu_0\epsilon_j\omega(\omega - i\tilde{\sigma}_j)$, $j = 0, 1, 2$, and $K_n = \epsilon_n/\epsilon_0$. This implies that

$$c_n = \frac{\sqrt{\omega(\omega - i\tilde{\sigma}_0)}}{\sqrt{K_n\omega(\omega - i\tilde{\sigma}_n)}},\ n = 1, 2,$$

$$C_{2,1} = +\frac{\sqrt{\omega(\omega - i\tilde{\sigma}_0)} - \sqrt{K_1\omega(\omega - i\tilde{\sigma}_1)}}{\sqrt{\omega(\omega - i\tilde{\sigma}_0)} + \sqrt{K_1\omega(\omega - i\tilde{\sigma}_1)}} - \frac{\sqrt{\omega(\omega - i\tilde{\sigma}_0)} - \sqrt{K_2\omega(\omega - i\tilde{\sigma}_2)}}{\sqrt{\omega(\omega - i\tilde{\sigma}_0)} + \sqrt{K_2\omega(\omega - i\tilde{\sigma}_2)}}, \quad (23)$$

$$e_{0,1}^{(0)}(x, z, t) = e_0^I(z, t) + e_{0,1}^{(R)}(z, t) - e_{s,0}^{(0)}(x, z, t) \quad (24)$$

and

$$e_{0,2}^{(0)}(x, z, t) = e_0^I(z, t) + e_{0,2}^{(R)}(z, t) + e_{s,0}^{(0)}(x, z, t). \quad (25)$$

Here $e_0^I(z, t)$ is given by (6); $e_{s,0}^{(0)}(x, z, t)$ is given by (15) with $A(\omega)$ given by (4) and $C_{2,1}$ given by (23), and for $n = 1, 2$,

$$e_{0,n}^{(R)}(z, t) = \frac{1}{\pi}\Re\left(\int_0^\infty A(\omega)\,\frac{c_n - 1}{c_n + 1}\,e^{i\omega t + i\kappa_0 z}\,d\omega\right). \quad (26)$$

Appendix D shows the integration of (26) similar to the analysis of equation (6).

Computation for a Nonconductive Upper Medium

Asymptotic Expression for $H_0^{(2)}$

For $z \neq 0$ and $|\omega z| >> 1$, we can replace $H_0^{(2)}$ by its asymptotic expression. *Sampaio and Popov* [1996] employed the asymptotic expression of $H_0^{(2)}$ to compute the acoustic scattering by a vertical fault for the regions $|x| = O(|z|)$ and $|x| << |z|$. They based their analysis on results obtained by *Popov and Camerlynck* [1996] and used the stationary point method [*Smirnov*, 1967] and Fresnel's integral. According to *Abramowitz and Stegun* [1968], their result can be applied in a straightforward manner to rewrite (15) in a form amenable to numerical computation for cases 1 and 2. For $|x| = O(|z|)$,

$$e_{s,0}^{(0)}(x, z, t) = \frac{1}{2\pi}\Re\left(-\int_0^\Omega \kappa_0 C_{2,1}A(\omega)e^{i\omega t}I(x, z, \omega)\,d\omega + \int_0^\Omega \kappa_0 C_{2,1}A(\omega)e^{i\omega t}I_{(sp)}(z, \omega)\,d\omega - \int_\Omega^\infty \kappa_0 C_{2,1}A(\omega)e^{i\omega t}I_{(ul)}(x, z, \omega)\,d\omega\right). \quad (27)$$

For $|x| << |z|$,

$$e_{s,0}^{(0)}(x, z, t) = \frac{1}{2\pi}\Re\left(-\int_0^\Omega \kappa_0 C_{2,1}A(\omega)e^{i\omega t}I(x, z, \omega)\,d\omega + \int_0^{\Omega^*} \kappa_0 C_{2,1}A(\omega)e^{i\omega t}I_{(sp)}(z, \omega)\,d\omega - \int_\Omega^{\Omega^*} \kappa_0 C_{2,1}A(\omega)e^{i\omega t}I_{(F)}(x, z, \omega)\,d\omega - \int_{\Omega^*}^\infty \kappa_0 C_{2,1}A(\omega)e^{i\omega t}I_{(F)}^*(x, z, \omega)\,d\omega\right). \quad (28)$$

In (27) and (28) we have added and subtracted the integral of $I_{(sp)}$, respectively, over the interval $(0, \Omega)$ and $(0, \Omega^*)$ to cancel out $e_{s,0}^{(0)}(0, z, t)$; and

$$I_{(sp)}(z, \omega) = \frac{e^{-i\kappa_0|z|}}{\kappa_0},$$

$$I_{(ul)}(x, z, \omega) = \frac{\sqrt{2\sqrt{x^2 + z^2}}}{x}\,\frac{ie^{i\left(\frac{\pi}{4} - \kappa_0\sqrt{x^2+z^2}\right)}}{\sqrt{\pi(\kappa_0)^3}},$$

$$I_{(F)}(x, z, \omega) = \frac{2\,e^{i\frac{\pi}{4}}}{\kappa_0\sqrt{\pi}}e^{-i\kappa_0|z|}\int_0^\psi e^{-i\tau^2}\,d\tau,$$

$$\psi = x\sqrt{\frac{|\kappa_0|}{2|z|}},$$

and

$$I_{(F)}^*(x, z, \omega) = \frac{i\sqrt{2|z|}\,e^{i\frac{\pi}{4}}}{x\sqrt{\pi(\kappa_0)^3}}\,e^{-i\kappa_0\left(|z| + \frac{x^2}{2|z|}\right)}.$$

Definition of the Parameters

We employed the following constant values: $c = 3 \times 10^8$ m/s; $a = 2 \times 10^7$ Hz; and $h = 30$ m. We computed the scattered electric field for three values of z: $z_1 = -9$ m, $z_2 = -21$ m, and $z_3 = -36$ m; 21 values of $0\,\text{m} \leq |x| \leq 10\,\text{m}$ at an interval of 0.5 m; and 76 values of $100\,\text{ns} \leq t \leq 250\,\text{ns}$ at an interval of 2 ns. We computed the numerical values of the exact function $I(x, z, \omega)$, employing the relationship between the Hankel function of the second kind, $H_0^{(2)}$, and the modified Bessel function of the second kind, K_0, via the following expression [*Abramowitz and Stegun*, 1968]:

$$I(x, z, \omega) = \frac{2i}{\pi} \int_0^x K_0\left(i\kappa_0 \sqrt{\eta^2 + z^2}\right) d\eta.$$

We followed the criterion of *Popov and Camerlynck* [1996] to define when ω is sufficiently large to apply high-frequency asymptotics. The corresponding values of ω are Ω and Ω^* in (27) and (28). For convenience we changed the variable of integration of the inverse Fourier transform from ω to ω/c. So in order to achieve 10% precision in the computation, we obtain from the Hankel function that we have to satisfy,

$$\frac{\Omega}{c} \geq \frac{1.25}{\sqrt{x^2 + z^2}}, \quad x = O(|z|),$$

and similarly for the Fresnel integral,

$$\frac{\Omega^*}{c} \geq 10\,\frac{|z|}{x^2}, \quad |x| << |z|.$$

This means that $\Omega/c = 1$, for $|z| = 5$ and any value of x, and that $\Omega^*/c = 800$ for $|z| = 20$ and $|x| = 0.5$ satisfy the condition of 10% precision. For the exact integration of the Hankel function we employed an interval of integration of 10^{-3}, and for the Fresnel integral we employed an interval of integration of $O(0.05)$. In the inverse Fourier transform we employed an interval of integration of 10^{-3} for $\omega/c < \Omega/c$, and of 10^{-2} for $\omega/c > \Omega/c$.

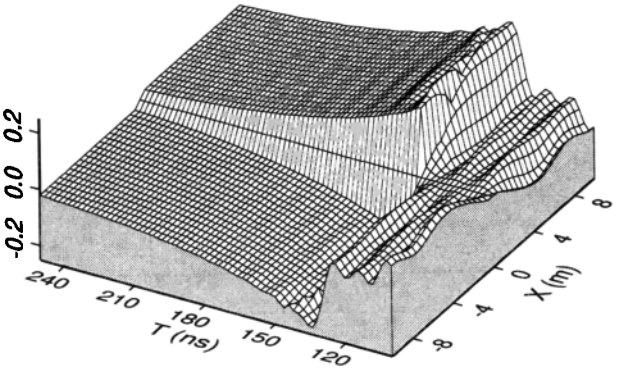

Figure 5. The vertical scale represents the variation of the ratio between the zero-order scattered electric field and the maximum value of the primary electric field with time and lateral distance to the fault for nonconductive media at $z = -9$ m.

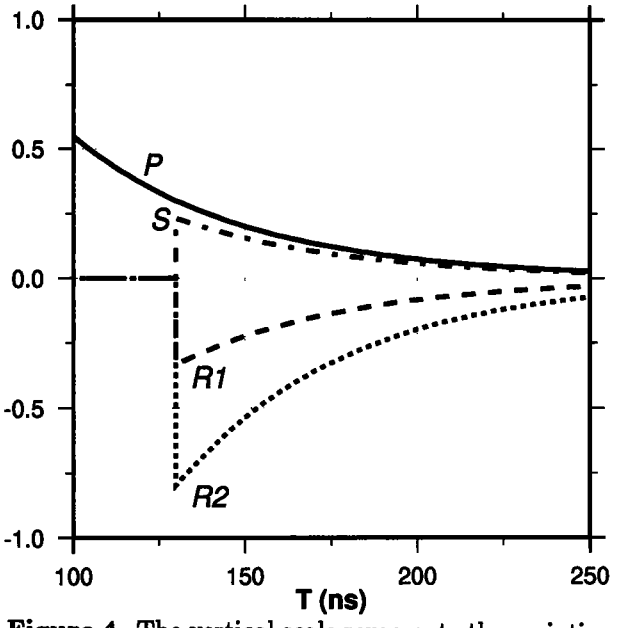

Figure 4. The vertical scale represents the variation of the ratio between the electric field components and the maximum value of the primary electric field for $z = -9$ m, $100\,\text{ns} \leq t \leq 250\,\text{ns}$, and nonconductive lower media: P, primary; R_1, reflected for $x < 0$; R_2, reflected for $x > 0$; and S, scattered for $x = 0^+$.

Nonconductive Lower Media

We computed the total field employing (14), (16), and (17) for $x = 0$. We computed the scattered field for $x \neq 0$ employing (27) and (28), both for $C_{2,1} = +7/15$. Equation (14) shows that $e_{s,0}^{(0)}(0, z_1, t) = 0$, for $t < 130$ ns, jumps to its maximum value equal to $+7/30$ at $t = 130^+$ ns, and decays exponentially to 0 with t, for $t > 130$ ns. A similar behavior happens to both $e_{s,0}^{(0)}(0, z_2, t)$, and $e_{s,0}^{(0)}(0, z_3, t)$, except that the reference values of time are $t = 170$ ns and $t = 220$ ns, respectively.

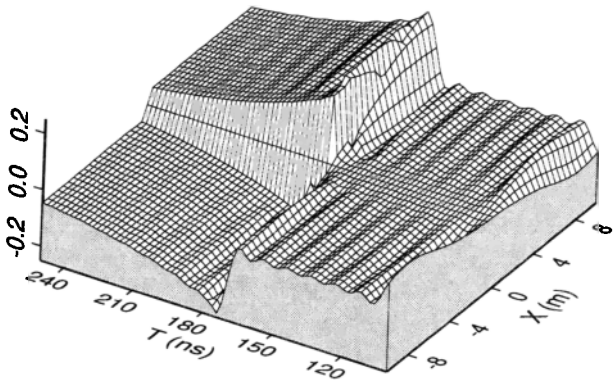

Figure 6. The vertical scale represents the variation of the ratio between the zero-order scattered electric field and the maximum value of the primary electric field with time and lateral distance to the fault for nonconductive media at $z = -21\,\mathrm{m}$.

Figure 4 presents the variation, for $z = z_1$, of the primary field, the reflected field for both sides of the fault, as well as the scattered field at $x = 0$. Notice the relative magnitude of the three components of the total field. Except for a very low lateral contrast between the two values of the dielectric permittivity, the scattered component cannot be neglected. However, it will be difficult to identify the scattered field component from the total field for measurements at a single point. Figures 5, 6, and 7 represent the variation of $e^{(0)}_{s,0}(x, z, t)$ for z equal to z_1, z_2, and z_3, respectively. We can observe that (1) the arrival and the propagation of the scattered wave front are well defined; (2) the wave front is better defined, varying smoothly and presenting a sharp jump for $|x|$ small; and (3) the definition of the wave front arrival is disturbed by a numerical noise with a frequency of about 100 MHz for $|x|$ large.

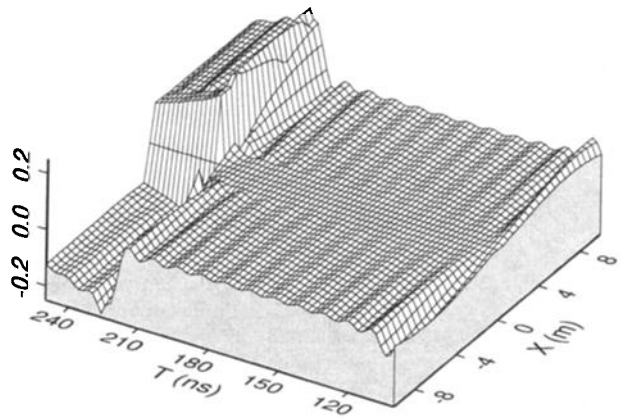

Figure 7. The vertical scale represents the variation of the ratio between the zero-order scattered electric field and the maximum value of the primary electric field with time and lateral distance to the fault for nonconductive media at $z = -36\,\mathrm{m}$.

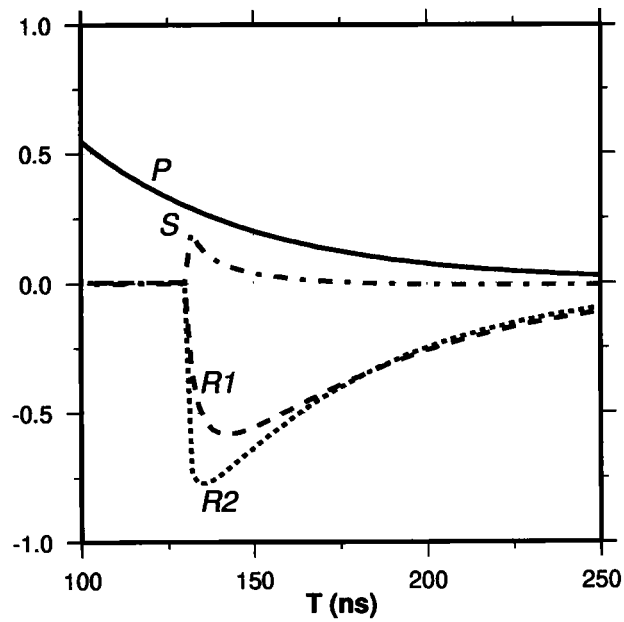

Figure 8. The vertical scale represents the variation of the ratio between the electric field components and the maximum value of the primary electric field for $z = -9\,\mathrm{m}$, $100\,\mathrm{ns} \leq t \leq 250\,\mathrm{ns}$, and conductive lower media. P, primary; R_1, reflected for $x < 0$; R_2, reflected for $x > 0$; and S, scattered for $x = 0^+$.

Conductive Lower Media

We computed the total field employing (20), (21), and (22), combined with (13) for $x = 0$. We computed the scattered field with (27) and (28) for $x \neq 0$, both for $C_{2,1}$ given by (19) employing the following constant values: $\tilde{\sigma}_1 = 36\pi \times 10^7\,\mathrm{S/F}$; $\tilde{\sigma}_2 = 36\pi \times 10^8\,\mathrm{S/F}$. Figure 8 presents the variation, for $z = z_1$, of the primary field, the reflected field for both sides of the fault, as well as the scattered field at $x = 0$. The behavior is similar to the one shown in Figure 4, except that the scattered component decays faster and the reflected components decay slower in this case. Figures 9, 10, and 11 present the variation of $e^{(0)}_{s,0}(x, z, t)$ for z equal to z_1, z_2, and z_3, respectively. We can observe that (1) the magnitude and the phase of the scattered field, as well as the arrival

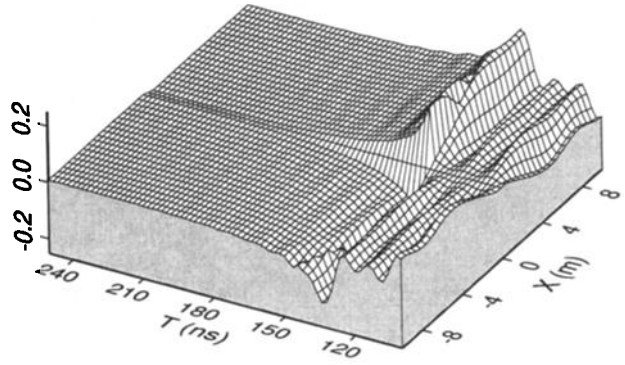

Figure 9. The vertical scale represents the variation of the ratio between the zero-order scattered electric field and the maximum value of the primary electric field with time and lateral distance to the fault for conductive lower media at $z = -9\,\mathrm{m}$.

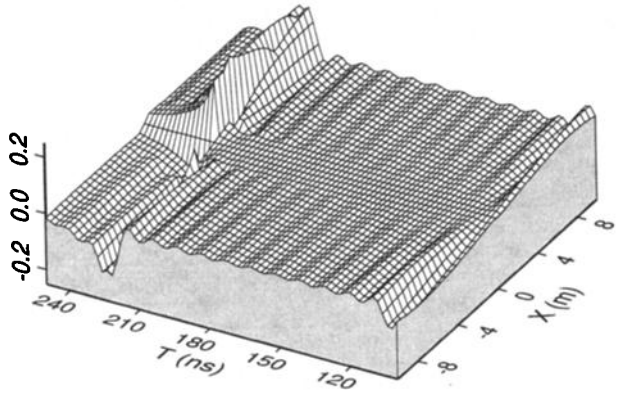

Figure 11. The vertical scale represents the variation of the ratio between the zero-order scattered electric field and the maximum value of the primary electric field with time and lateral distance to the fault for conductive lower media at $z = -36\,\mathrm{m}$.

and the propagation of the wave front, are well defined; (2) the wave front is better defined, varying smoothly and having a sharp jump for $|\ x\ | << |\ z\ |$; and (3) the wave front is less abrupt for $|\ x\ | = O(z)$ and presents the same numerical noise oscillating at about 100 MHz. Comparing Figures 9, 10, and 11 with Figures 5, 6, and 7, respectively, we see that in the present case, the field has a smaller magnitude and decays faster in time. Otherwise, they present similar behavior.

Three Conductive Media

To determine the primary and the reflected fields, we employ equations (A2), (A3), (A4), (D6), (D7), and (D8). Notice that if $a > \tilde{\sigma}_0/2$, both (A4) and (D8) do not contribute to the fields, and the integrals (A3) and (D7) are no longer Cauchy principal values. The contributions of (A2) and (D6) diffuse away with time very rapidly: for seawater ($\tilde{\sigma}_0 = \frac{4}{3}\pi \times 10^9\,\mathrm{S/F}$), they are negligible for $t > 5\,\mathrm{ns}$; for $\tilde{\sigma}_0$ 10 times smaller, they are negligible for $t > 50\,\mathrm{ns}$. So the main contribution comes from (A4) and (D8) for $a < \tilde{\sigma}_0/2$, and from (A3) and (D7) for $a > \tilde{\sigma}_0/2$. Notice also that Appendix B shows that the propagation velocity (not the phase velocity) does not depend on the conductivity of the medium. To determine the scattered field, we can employ the same path of integration of Appendix A and D on (13) and (15). So the main contribution will come from the integral around the pole $\omega = ia$, for $a < \tilde{\sigma}_0/2$, and from the integral along the branch cut from $\omega = 0$ to $\omega = i\frac{\tilde{\sigma}_0}{2}$ for $a > \tilde{\sigma}_0/2$.

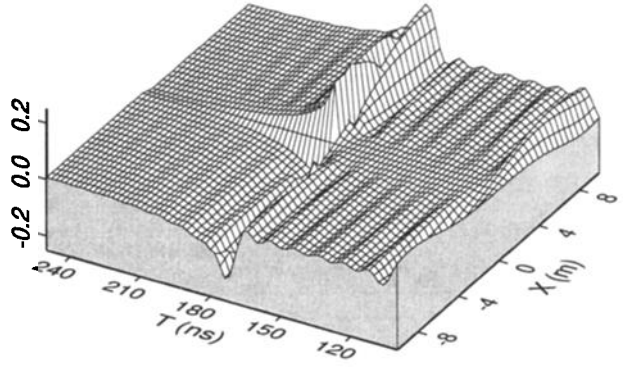

Figure 10. The vertical scale represents the variation of the ratio between the zero-order scattered electric field and the maximum value of the primary electric field with time and lateral distance to the fault for conductive lower media at $z = -21\,\mathrm{m}$.

Conclusion

We have successfully adapted to the time domain an exact and complete solution of the scattering of electromagnetic plane waves by two quarter spaces. This result can be employed to check the accuracy of results of forward modeling obtained by other techniques. The result obtained with the zero-order approximation of the solution is useful because it defines the amplitude and the phase of the scattered field besides the shape of the wave front. However, refinement of the computation and higher-order approximations are necessary to improve the accuracy, to decrease the numerical noise, and to consider the variations of ϵ and μ in the conductive media.

Appendix A: Integral for the Incident Wave in a Conductive Medium

Equation (6) can be expressed as

$$e_0^I(z,t) = \frac{1}{2\pi}\int_{-\infty}^{\infty} \frac{N(\omega)}{a+i\omega} e^{-i\kappa_0(z+h)+i\omega t}\, d\omega, \quad \text{(A1)}$$

where $\kappa_0 = \sqrt{\mu_0\epsilon_0}\,\tilde{\kappa}_0$, $\tilde{\kappa}_0 = \sqrt{\omega(\omega - i\tilde{\sigma}_0)}$, and

$$N(\omega) = \frac{2\mu_0\omega\sqrt{\mu_v\epsilon_v}}{(\mu_v\kappa_0 + \mu_0\omega\sqrt{\mu_v\epsilon_v})}.$$

Let us set the branch cut on the ω plane between $\omega = 0$ and $\omega = i\tilde{\sigma}_0$. Let us also fix the regular branch of $\tilde{\kappa}_0(\omega)$ by the condition that $\Im(\tilde{\kappa}_0) = 0$ on the cut line. It yields

$$\tilde{\kappa}_0 = |\omega(\omega - i\tilde{\sigma}_0)|^{1/2} \exp\left(i\frac{\arg(\omega) + \arg(\omega - i\tilde{\sigma}_0)}{2}\right).$$

This is indeed so, because $\arg(\tilde{\kappa}_0) = 0$ on the right-hand side of the cut line and $\arg(\tilde{\kappa}_0) = -\pi$ on the left-hand side of the cut line. Outside the cut line, $\Im(\tilde{\kappa}_0) > 0$ for $\Im(\omega) > \tilde{\sigma}_0/2$, $\Im(\tilde{\kappa}_0) = 0$ for $\Im(\omega) = \tilde{\sigma}_0/2$, and $\Im(\tilde{\kappa}_0) < 0$ for $\Im(\omega) < \tilde{\sigma}_0/2$.

For $t < (z+h)\sqrt{\mu_0\epsilon_0}$ we can close the contour of integration in the lower half plane of ω, resulting in $e_0^I(z,t) = 0$. So it is causal. For $t > (z+h)\sqrt{\mu_0\epsilon_0}$ we deform the path of integration as shown in Figure A1, where we assume that $a < \tilde{\sigma}_0/2$. Therefore

$$e_0^I(z,t) = I_1 + I_2 + I_3,$$

where I_1 is the integral along the straight line $\omega = \eta + i\tilde{\sigma}_0/2$, $-\infty < \eta < +\infty$; I_2 is the integral along both sides of the branch cut $\omega = i\xi$, $0 \le \xi \le \tilde{\sigma}_0/2$; and I_3 is the integral around the pole $\omega = ia$.

Since $\kappa_0 = sgn(\eta)|\kappa_0|$ on the straight line $\Im(\omega) = \tilde{\sigma}_0/2$, then $N(\omega)$ will vary accordingly. Therefore we

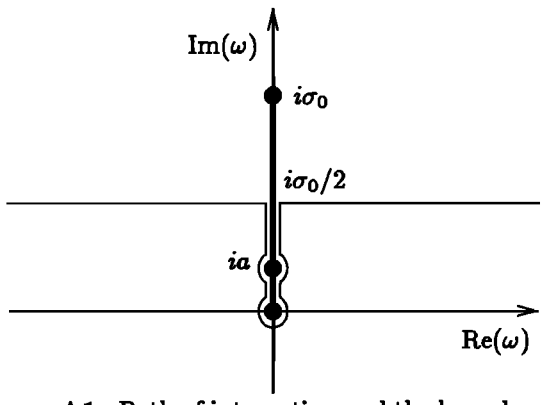

Figure A1. Path of integration and the branch cuts of the ω plane for the integrals (A1), (D1), and (D5).

can show that

$$I_1 = \frac{e^{-\frac{\tilde{\sigma}_0}{2}t}}{2\pi}\int_0^{\infty}\left\{\frac{N(-\eta + i\frac{\tilde{\sigma}_0}{2})}{a - \frac{\tilde{\sigma}_0}{2} - i\eta} e^{+i|\kappa_0|(z+h)-i\eta t} + \frac{N(+\eta + i\frac{\tilde{\sigma}_0}{2})}{a - \frac{\tilde{\sigma}_0}{2} + i\eta} e^{-i|\kappa_0|(z+h)+i\eta t}\right\} d\eta. \quad \text{(A2)}$$

Let $\kappa_0^{(+)}(\xi) = +\sqrt{\mu_0\epsilon_0}\sqrt{\xi(\tilde{\sigma}_0 - \xi)}$ and $\kappa_0^{(-)}(\xi) = -\sqrt{\mu_0\epsilon_0}\sqrt{\xi(\tilde{\sigma}_0 - \xi)}$ be the values of κ_0 on the right-hand side and on the left-hand side of the cut line, respectively, for $0 \le \xi \le \tilde{\sigma}_0/2$, $\xi \ne a$. Therefore

$$N^{(\pm)}(i\xi) = \frac{2i\mu_0\xi\sqrt{\mu_v\epsilon_v}}{(\mu_v\kappa_0^{(\pm)}(\xi) + i\mu_0\xi\sqrt{\mu_v\epsilon_v})},$$

and we can show that

$$I_2 = \frac{1}{2\pi}\int_0^{\frac{\tilde{\sigma}_0}{2}} \frac{ie^{-\xi t}}{a-\xi}\left\{-N^{(-)}(i\xi)\, e^{-i\kappa_0^{(-)}(z+h)} + N^{(+)}(i\xi)\, e^{-i\kappa_0^{(+)}(z+h)}\right\} d\xi. \quad \text{(A3)}$$

Applying the theorem of residues, it is straightforward to show that for $\xi = a$,

$$I_3 = \frac{1}{2}e^{-at}\left\{N^{(-)}(ia)\, e^{-i\kappa_0^{(-)}(z+h)} + N^{(+)}(ia)\, e^{-i\kappa_0^{(+)}(z+h)}\right\}. \quad \text{(A4)}$$

Appendix B: On the Wave Front for the Incident Wave

It is necessary to search whether it is possible to close the contour of integration in the lower half plane of ω for values of $z+h$ and t such that $\Im(\kappa_0(z+h) - \omega t) < 0$. Similarly to Jordan's lemma, we have to study the integral along the semicircle $\omega = \rho e^{i\phi}$, $-\pi \le \phi \le 0$. Developing the exponential term in (A1) along that semicircle, we have

$$-i\kappa_0(z+h) + i\omega t = -i\rho e^{i\phi}\left((z+h)\sqrt{\mu_0\epsilon_0(1-\xi)} - t\right),$$

$$\xi = \frac{\tilde{\sigma}_0}{\rho}e^{i(\frac{\pi}{2}-\phi)},$$

and therefore

$$\left|\exp\left\{-i\rho e^{i\phi}\left((z+h)\sqrt{\mu_0\epsilon_0(1-\xi)} - t\right)\right\}\right| = exp\left\{\rho\cos(\phi)W''(z+h)\sqrt{\mu_0\epsilon_0} + \rho\sin(\phi)(W'(z+h)\sqrt{\mu_0\epsilon_0} - t)\right\} \quad \text{(B1)}$$

where

$$W' = |\sqrt{1-\xi}| \cos\frac{\arg(1-\xi)}{2},$$

and

$$W'' = |\sqrt{1-\xi}| \sin\frac{\arg(1-\xi)}{2}.$$

It can be shown that $W'' \cos(\phi) \leq 0$ for $-\pi < \phi < 0$. Now suppose that on this same interval of ϕ the following equation holds: $W'(z+h)\sqrt{\mu_0\epsilon_0} - t > 0$. Then

$$W'(z+h)\sqrt{\mu_0\epsilon_0} - t \geq \min_{\phi}(W')(z+h)\sqrt{\mu_0\epsilon_0} - t,$$

and it is clear that $\min_\phi(W') = W'(\phi = 0) = W'(\phi = -\pi) = W'_{\min}$. Obviously, this minimum depends upon ρ. Taking this into account, we arrive at the following estimation:

$$\exp(\rho\sin(\phi)(W'(z+h)\sqrt{\mu_0\epsilon_0} - t)) \leq$$

$$\exp(\rho\sin(\phi)(W'_{\min}(z+h)\sqrt{\mu_0\epsilon_0} - t)).$$

So it is evident that in the limit $\rho \to \infty$ along the semicircle $-\pi \leq \phi \leq 0$, the integral (A1) vanishes and

$$\lim_{\rho\to\infty}\left(W'_{\min}(z+h)\sqrt{\mu_0\epsilon_0} - t\right) = (z+h)\sqrt{\mu_0\epsilon_0} - t,$$

and therefore the singularity of the integral is on the wave front for $(z+h)\sqrt{\mu_0\epsilon_0} - t = 0$.

Appendix C: Analytical Properties of N(ω)

Let us rewrite $N(\omega)$ in the following form:

$$N(\omega) = \frac{2\omega}{B\sqrt{\omega(\omega - i\tilde{\sigma}_0)} + \omega},$$

where $B = \sqrt{\frac{\mu_v\epsilon_0}{\mu_0\epsilon_v}}$. The denominator is zero when the following equation is satisfied:

$$B\sqrt{\omega(\omega - i\tilde{\sigma}_0)} = -\omega. \qquad \text{(C1)}$$

So the denominator of $N(\omega)$ is zero for $\omega_1 = \rho e^{i\phi} = 0$. However, $N(\omega) \to 0$ as $\sqrt{\rho}$ with $\rho \to 0$. Thus $\omega_1 = 0$ is a regular point of $N(\omega)$. The second root, ω_2, of equation (C1) is

$$\omega_2 = i\tilde{\sigma}_0\frac{B^2}{B^2-1}.$$

Therefore $\Re(\omega_2) = 0$ and, if we assume that $B^2 - 1 > 0$, then $\Im(\omega_2) > \tilde{\sigma}_0$. Let us examine whether ω_2 is located on that sheet of the surface of Rieman where the regular branch of $\sqrt{\omega(\omega - i\tilde{\sigma}_0)}$ is defined. Above the line $\Im(\omega) = \tilde{\sigma}_0/2$, $\Im(\sqrt{\omega(\omega - i\tilde{\sigma}_0)}) > 0$, and $\Im(-\omega) < 0$. This contradiction proves that ω_2 is not located on the sheet of the surface of Rieman under consideration. The same contradiction occurs for $B^2 - 1 < 0$. Therefore $N(\omega)$ does not interfere with the development of the integral for the incident wave. Let us finally express $N(\omega)$ on both sides of the branch cut line $\omega = i\xi$, $0 \leq \xi \leq \tilde{\sigma}_0$:

$$N^-(\omega) = \frac{2i\xi}{-B\sqrt{\xi(\tilde{\sigma}_0 - \xi)} + i\xi},$$

$$N^+(\omega) = \frac{2i\xi}{+B\sqrt{\xi(\tilde{\sigma}_0 - \xi)} + i\xi}.$$

Appendix D: Integrals for the Reflected Waves

Nonconductive Upper Medium

We may write equation (22) for $n = 1, 2$ in the following form:

$$e^{(R)}_{0,n}(z,t) = \frac{1}{2\pi}\int_{-\infty}^{+\infty}\frac{\omega - \sqrt{\omega(\omega - i\tilde{\sigma}_n)}}{\omega + \sqrt{\omega(\omega - i\tilde{\sigma}_n)}}\frac{e^{i\omega t^+}}{a + i\omega}\,d\omega. \qquad \text{(D1)}$$

Let us set the branch cut on the ω plane between $\omega = 0$ and $\omega = i\tilde{\sigma}_n$. For $t^+ < 0$ we can close the contour of integration in the lower half plane of ω and therefore $e^{(R)}_{0,n}(z,t) = 0$, and it is causal. For $t^+ > 0$ we deform the path of integration as shown in Figure A1, where we assume that $a < \tilde{\sigma}_n/2$. Therefore

$$e^{(R)}_{0,n}(z,t) = I_4 + I_5 + I_6,$$

where I_4 is the integral along the straight line $\omega = \eta + i\tilde{\sigma}_n/2$, $-\infty < \eta < +\infty$; I_5 is the integral along both sides of the branch cut $\omega = i\xi$, $0 \leq \xi \leq \tilde{\sigma}_n/2$; and I_6 is the integral around the pole $\omega = ia$.

$$I_4 = \frac{\tilde{\sigma}_n e^{-\frac{\tilde{\sigma}_n}{2}t^+}}{\pi}\int_0^{\infty}\frac{\alpha\left(\eta\cos(\eta t^+) + \beta\sin(\eta t^+)\right)}{\left((\eta+\alpha)^2 + (\frac{\tilde{\sigma}_n}{2})^2\right)\left(\eta^2 + \beta^2\right)}\,d\eta, \qquad \text{(D2)}$$

$$\alpha = \sqrt{\eta^2 + (\frac{\tilde{\sigma}_n}{2})^2},$$

$$\beta = \frac{\tilde{\sigma}_n}{2} - a,$$

$$I_5 = \frac{2}{\tilde{\sigma}_n \pi} \int_0^{\frac{\tilde{\sigma}_n}{2}} \frac{\sqrt{\xi(\tilde{\sigma}_n - \xi)}}{\xi - a} e^{-\xi t^+} d\xi, \qquad \text{(D3)}$$

$$I_6 = -e^{-at^+} \frac{\tilde{\sigma}_n - a}{\tilde{\sigma}_n}. \qquad \text{(D4)}$$

Conductive Upper Medium

Let us express equation (26) for $n = 1, 2$ as

$$e_{0,n}^{(R)}(z,t) = \frac{1}{2\pi} \int_{-\infty}^{\infty} \frac{M_n(\omega)}{a + i\omega} e^{i\kappa_0(z-h)+i\omega t} d\omega, \quad \text{(D5)}$$

where

$$M_n(\omega) = \frac{2\mu_0\omega\sqrt{\mu_v\epsilon_v}}{(\mu_v\kappa_0 + \mu_0\omega\sqrt{\mu_v\epsilon_v})} \times \frac{\sqrt{\omega(\omega - i\tilde{\sigma}_0)} - \sqrt{K_n\omega(\omega - i\tilde{\sigma}_n)}}{\sqrt{\omega(\omega - i\tilde{\sigma}_0)} + \sqrt{K_n\omega(\omega - i\tilde{\sigma}_n)}},$$

$\kappa_n = \sqrt{\mu_0\epsilon_n}\,\tilde{\kappa}_n$, and $\tilde{\kappa}_n = \sqrt{\omega(\omega - i\tilde{\sigma}_n)}$. If we choose the regular branch of $\tilde{\kappa}_n(\omega)$ exactly as for the incident wave, every branch cut starts at $\omega = 0$ and ends at $\omega = i\tilde{\sigma}_n$. So there are no singularities in the lower half plane of the ω plane. For $t < (h-z)\sqrt{\mu_0\epsilon_0}$ we can close the contour of integration in the lower half plane of ω, resulting in $e_{0,n}^{(R)}(z,t) = 0$. So it is causal. For $t > (h-z)\sqrt{\mu_0\epsilon_0}$ the contour of integration can be deformed exactly like for the incident wave as shown in Figure A1, and

$$e_{0,n}^{(R)}(z,t) = I_7 + I_8 + I_9.$$

$$I_7 = \frac{1}{2\pi} e^{-\frac{\tilde{\sigma}_0}{2}t} \int_0^{\infty} \left\{ \frac{M_n(-\eta + i\frac{\tilde{\sigma}_0}{2})}{a - \frac{\tilde{\sigma}_0}{2} - i\eta} e^{-i|\kappa_0|(z-h)-i\eta t} + \frac{M_n(+\eta + i\frac{\tilde{\sigma}_0}{2})}{a - \frac{\tilde{\sigma}_0}{2} + i\eta} e^{+i|\kappa_0|(z-h)+i\eta t} \right\} d\eta. \quad \text{(D6)}$$

$$I_8 = \frac{1}{2\pi} \int_0^{\frac{\tilde{\sigma}_0}{2}} \frac{ie^{-\xi t}}{a - \xi} \left\{ -M_n^{(-)}(i\xi)\, e^{+i\kappa_0^{(-)}(z-h)} + M_n^{(+)}(i\xi)\, e^{+i\kappa_0^{(+)}(z-h)} \right\} d\xi. \qquad \text{(D7)}$$

$$I_9 = \frac{1}{2} e^{-at} \left\{ M_n^{(-)}(ia)\, e^{+i\kappa_0^{(-)}(z-h)} + M_n^{(+)}(ia)\, e^{+i\kappa_0^{(+)}(z-h)} \right\}. \qquad \text{(D8)}$$

Acknowledgments. This work has been funded by CNPq and PETROBRAS. We acknowledge the suggestions of H. Sato.

References

Abramowitz, M., and I. Stegun (Eds.), *Handbook of Mathematical Functions With Formulas, Graphs and Mathematical Tables*, Appl. Math. Ser. 55, Natl. Inst. of Stand. and Technol., U. S. Dep. of Commer., Washington, D. C., 1968.

Erdélyi, A. (Ed.), *Tables of Integral Transforms*, vol. I, McGraw-Hill, New York, 1954.

Popov, M. M., and C. Camerlynck, Second term of the ray series and validity of the ray theory, *J. Geophys. Res., 101*(1), 817-826, 1996.

Sampaio, E. S., and J. T. Fokkema, Scattering of monochromatic acoustic and electromagnetic plane waves by two quarter spaces, *J. Geophys. Res., 97*(B2), 1953-1963, 1992.

Sampaio, E. S., and M. M. Popov, Time domain scattering of acoustic plane waves by vertical faults, *Pure Appl. Geophys., 148*(1/2), 95-112, 1996.

Smirnov, V. I., *A Course of Higher Mathematics*, vol. III, Pergamon, Tarrytown, N. Y., 1967.

Sommerfeld, A., Mathematical theory of diffraction (in German), *Math. Ann., 47*, 317-374, 1896.

M. M. Popov, V. A. Steklov Mathematical Institute, Fontanka 27, 191011, St. Petersburg, Russia. (e-mail: mpopov@.pdmi.ras.ru)

E. E. S. Sampaio, PPPG/UFBA, Rua Barão de Geremoabo s/n, Instituto de Geociências sala 308-C, 40170-290, Salvador-Bahia, Brazil. (e-mail: edson@pppg.ufba.br)

(Received June 25, 1996; revised October 8, 1996; accepted October 18, 1996.)